*Materials Transactions*, Vol. 47, No. 10 (2006) pp. 2480 to 2488


# Evaluation of Interdiffusion in Liquid Phase during Reactive Diffusion between Cu and Al

Yasuhiko Tanaka[1] and Masanori Kajihara[2,*]

[1]*Graduate School, Tokyo Institute of Technology, Yokohama 226-8502, Japan*
[2]*Department of Materials Science and Engineering, Tokyo Institute of Technology*

Using Cu/Al diffusion couples initially composed of pure Cu and Al, the reactive diffusion in the binary Cu–Al system was experimentally examined in a previous study. The diffusion couple was isothermally annealed in the temperature range of $T = 973$–$1073$ K. Due to annealing, compound layers of the $\beta$, $\gamma$ and $\varepsilon$ phases are formed between the Cu-rich solid ($\alpha$) phase and the Al-rich liquid ($L$) phase, and the $L/\varepsilon$ interface migrates towards the $\varepsilon$ phase. At each annealing time, the migration distance of the $L/\varepsilon$ interface is much greater than the total thickness of the compound layers. Furthermore, there exists the parabolic relationship between the migration distance and the annealing time. This means that the migration of the interface is controlled by the volume diffusion in the $L$ phase. The mathematical model for the interface migration controlled by volume diffusion was used in order to analyze quantitatively the migration rate of the interface. Through the analysis, the interdiffusion coefficient $D$ of the $L$ phase was evaluated to be $1.24 \times 10^{-9}$, $2.91 \times 10^{-9}$ and $3.62 \times 10^{-9}$ m$^2$/s at $T = 973$, 1023 and 1073 K, respectively. Expressing the temperature dependence of $D$ as $D = D_0 \exp(-Q/RT)$, values of $D_0 = 1.42 \times 10^{-4}$ m$^2$/s and $Q = 93.5$ kJ/mol were obtained by the least-squares method. According to the analysis, the interdiffusion coefficient is much greater for the $L$ phase than for the solid phases. Consequently, the $L/\varepsilon$ interface migrates towards the $\varepsilon$ phase, and the migration rate of the interface is much greater than the overall growth rate of the compound layers. [doi:10.2320/matertrans.47.2480]

(Received June 19, 2006; Accepted August 21, 2006; Published October 15, 2006)

***Keywords:*** *intermetallic compounds, bulk diffusion, analytical methods, reactive diffusion, kinetics*

## 1. Introduction

There are many binary alloy systems where intermetallic compounds appear as stable phases.[1)] Reactive diffusion has been experimentally studied for such alloy systems by many investigators.[2–31)] In those experiments, diffusion couples were prepared from different pure metals or alloys and then isothermally annealed at appropriate temperatures. After annealing, some of the stable compounds were observed as layers at the interface in the diffusion couple. When the reactive diffusion is controlled by volume diffusion, the total thickness $l$ of the compound layers is expressed as a function of the annealing time $t$ by the parabolic relationship $l^2 = Kt$. Here, $K$ is the parabolic coefficient. The parabolic relationship may be believed to hold good in many alloy systems. However, the volume diffusion is not necessarily the rate-controlling process of reactive diffusion for all the alloy systems.

The reactive diffusion in the binary Au–Sn system was experimentally observed using Sn/Au/Sn diffusion couples in previous studies.[15–17)] The diffusion couple was isothermally annealed at temperatures between $T = 393$ and 473 K. Due to annealing, compound layers composed of AuSn, $AuSn_2$ and $AuSn_4$ are produced at the Au/Sn interface in the diffusion couple. The total thickness of the compound layers is proportional to a power function of the annealing time, and the exponent of the power function is 0.48, 0.42 and 0.36 at $T = 393$, 433 and 473 K, respectively. Consequently, the exponent is smaller than 0.5 at most of the annealing temperatures, and thus the parabolic relationship does not hold good for the reactive diffusion in the binary Au–Sn system. This means that grain boundary diffusion as well as volume diffusion contributes to the rate-controlling process and grain growth occurs at certain rates in the compound layers. Such a mixed rate-controlling process was recognized also for the reactive diffusion in the binary Ag–Sn,[18)] Ni–Sn[19)] and Cu–Sn[20)] systems.

For the binary Fe–Al system, the reactive diffusion was experimentally observed using Al/Fe/Al diffusion couples in a previous study.[21)] Owing to isothermal annealing at $T = 823$–$913$ K, a single compound layer of $Fe_2Al_5$ is formed at the interface in the diffusion couple, and grows according to the parabolic relationship. This indicates that the growth of the $Fe_2Al_5$ layer is controlled by volume diffusion. This type of rate-controlling process was observed also for the binary Pd–Sn system.[22)] In this case, compound layers consisting of $PdSn_4$, $PdSn_3$ and $PdSn_2$ are formed at $T = 433$ K, but those composed of only $PdSn_4$ and $PdSn_3$ are produced at $T = 453$ and 473 K. At all these temperatures, there exists the parabolic relationship between the total thickness of the Pd–Sn compound layers and the annealing time. As previously mentioned, however, the parabolic relationship does not hold good for the binary Au–Sn, Ag–Sn, Cu–Sn and Ni–Sn systems. Therefore, the rate-controlling process of reactive diffusion varies depending on the alloy system.

The kinetics of the reactive diffusion controlled by volume diffusion was theoretically analyzed using a mathematical model in a previous study.[32)] In the theoretical analysis, a hypothetical binary alloy system composed of two primary solid solution phases and one intermetallic compound was considered in order to evaluate the growth rate of the compound in various semi-infinite diffusion couples initially consisting of the two primary solid solution phases with different solubility ranges and interdiffusion coefficients. The mathematical model was also used to analyze numerically the relationship between the temperature dependence of the interdiffusion in each phase and the kinetics of the reactive diffusion.[33–35)] As mentioned earlier, the single compound

*Corresponding author, E-mail: kajihara@materia.titech.ac.jp

layer of $Fe_2Al_5$ is formed during reactive diffusion in the binary Fe–Al system.[21] Furthermore, the growth of the $Fe_2Al_5$ layer is controlled by volume diffusion. Thus, the mathematical model[32] was used to analyze numerically the growth behavior of the $Fe_2Al_5$ layer in a previous study.[36] Through the analysis, the interdiffusion coefficient of $Fe_2Al_5$ was evaluated quantitatively.

Recently, the reactive diffusion in the binary Cu–Al system was experimentally observed using Cu/Al diffusion couples by the present authors.[28] In that experiment, the diffusion couple was isothermally annealed in the temperature range between $T = 973$ and 1073 K. In this temperature range, Cu is solid, but Al is liquid. During annealing, compound layers composed of the $\beta$, $\gamma$ and $\varepsilon$ phases are formed at the interface between the Cu-rich solid ($\alpha$) phase and the Al-rich liquid ($L$) phase. The total thickness $l$ of the compound layers is proportional to a power function of the annealing time $t$, and the exponent of the power function is 0.15, 0.41 and 0.33 at $T = 973$, 1023 and 1073 K, respectively. Hence, the exponent is smaller than 0.5 at all the annealing temperatures. As a consequence, like the binary Au–Sn,[15–17] Ag–Sn,[18] Ni–Sn[19] and Cu–Sn[20] systems, grain boundary diffusion as well as volume diffusion contributes to the rate-controlling process and grain growth takes place at certain rates in the compound layers for the binary Cu–Al system. Unfortunately, however, the mathematical model[32] mentioned above cannot be applicable to such a rate-controlling process. On the other hand, the interface between the $L$ and $\varepsilon$ phases migrates towards the $\varepsilon$ phase during reactive diffusion in the binary Cu–Al system. Furthermore, the migration distance $w$ of the $L/\varepsilon$ interface is much greater than the total thickness $l$ of the compound layers, and the square of the migration distance $w$ is proportional to the annealing time $t$. This means that interdiffusion occurs more remarkably in the $L$ phase than in the $\alpha$, $\beta$, $\gamma$ and $\varepsilon$ phases, and the migration of the $L/\varepsilon$ interface is controlled by the volume diffusion in the $L$ phase. In the present study, the interdiffusion coefficient $D$ for volume diffusion in the $L$ phase of the binary Cu–Al system was quantitatively evaluated from the experimental result for the migration behavior of the $L/\varepsilon$ interface.

## 2. Experimental Summary

As mentioned in Section 1, the reactive diffusion in the binary Cu–Al system was experimentally observed in a previous study.[28] In that experiment, columnar diffusion couples consisting of pure solid Cu and pure liquid Al were isothermally annealed in the temperature range between $T =$ 973 and 1073 K. Here, the diameter is 8 and 8.5 mm for Cu and Al, respectively, and the initial thickness is 5 and 4.8 mm for Cu and Al, respectively. The interface between Cu and Al is flat and perpendicular to the columnar axis. During annealing, compound layers of the $\beta$, $\gamma$ and $\varepsilon$ phases are produced at the interface in the Cu/Al diffusion couple. According to a recent phase diagram in the binary Cu–Al system,[37] the $\beta$, $\gamma$ and $\varepsilon$ phases are the only stable compounds at $T = 973$–1073 K. At these temperatures, the $\beta$ and $\varepsilon$ phases are in equilibrium with the Cu-rich solid ($\alpha$) and Al-rich liquid ($L$) phases, respectively. Consequently, all

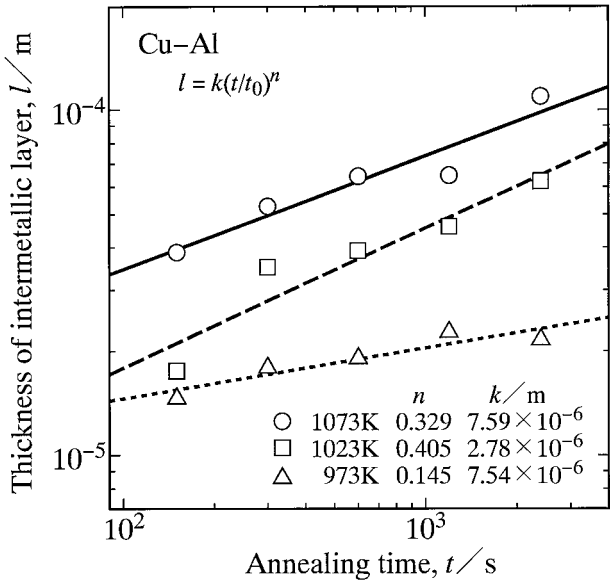


Fig. 1 The total thickness $l$ of the intermetallic layer versus the annealing time $t$ shown as open triangles, squares and circles at $T = 973$, 1023 and 1073 K, respectively. Straight lines indicate the calculations from eq. (1).

the stable phases were recognized in the annealed Cu/Al diffusion couple. The layer composed of the $\beta$, $\gamma$ and $\varepsilon$ phases is hereafter called the intermetallic layer. The total thickness $l$ of the intermetallic layer was determined experimentally. The values of $l$ are plotted against the annealing time $t$ in Fig. 1. In this figure, the ordinate and the abscissa show the logarithms of $l$ and $t$, respectively. Furthermore, open triangles, squares and circles indicate the results of $T = 973$, 1023 and 1073 K, respectively. As can be seen, the thickness $l$ monotonically increases with increasing annealing time $t$. The plotted points at each annealing temperature are located well on a straight line. This yields that the thickness $l$ is expressed as a power function of the annealing time $t$ by the equation

$$l = k(t/t_0)^n. \tag{1}$$

Here, $t_0$ is unit time, 1 s. It is adopted to make the argument $t/t_0$ of the power function dimensionless. The proportionality coefficient $k$ has the same dimension as the thickness $l$, but the exponent $n$ is dimensionless. From the plotted points in Fig. 1, the values of $k$ and $n$ were determined by the least-squares method. The determined values are shown in Fig. 1. Using these values of $k$ and $n$, the thickness $l$ was calculated as a function of the annealing time $t$ from eq. (1). The results of $T = 973$, 1023 and 1073 K are indicated as dotted, dashed and solid lines, respectively, in Fig. 1. At each experimental annealing time, the thickness $l$ monotonically increases with increasing annealing temperature $T$. Thus, the higher the annealing temperature $T$ is, the faster the intermetallic layer grows.

According to the result in Fig. 1, the exponent $n$ is 0.15, 0.41 and 0.33 at $T = 973$, 1023 and 1073 K, respectively. If the volume diffusion of the constituent elements in each phase is the rate-controlling process for the growth of the intermetallic layer, $n$ is equal to 0.5. On the other hand, the growth will be controlled by the grain boundary diffusion

along grain boundaries with a finite thickness in the intermetallic layer at annealing temperatures where the volume diffusion is much slower than the grain boundary diffusion. When grain growth occurs in the intermetallic layer, the volume fraction of the grain boundaries monotonically decreases with increasing annealing time. Such decrease in the volume fraction causes the decrement of the effective cross-section, and decelerates the grain boundary diffusion. As a result, $n$ becomes smaller than 0.5.[38] When the grain growth occurs very sluggishly, the volume fraction of the grain boundaries remains almost constant during annealing. In such a case, the effective cross-section for the grain boundary diffusion hardly varies, and thus $n$ is almost equal to 0.5. According to the result in Fig. 1, $n$ is smaller than 0.5 at all the annealing temperatures. Consequently, it is concluded that the grain boundary diffusion as well as the volume diffusion contributes to the rate-controlling process and the grain growth occurs at certain rates in the intermetallic layer for the reactive diffusion in the binary Cu–Al system at $T = 973$–$1073$ K.

During growth of the intermetallic layer, the interface between the $L$ and $\varepsilon$ phases migrates towards the $\varepsilon$ phase. Subtracting the thicknesses of the intermetallic layer and the $\alpha$ phase from the initial thickness of the $\alpha$ phase, we can determine the migration distance $w$ of the $L/\varepsilon$ interface at each annealing time.[28] The values of $w$ are plotted against the annealing time $t$ in Fig. 2. In this figure, the ordinate indicates the migration distance $w$, and the abscissa shows the square root of the annealing time $t$. Open triangles, squares and circles indicate the results of $T = 973$, 1023 and 1073 K, respectively. Although the open triangles are rather scattered, most of the plotted points lie well on the corresponding straight line. This means that the parabolic relationship holds good between $w$ and $t$ as follows.

$$w^2 = Kt \tag{2}$$

Here, $K$ is the parabolic coefficient with a dimension of $m^2/s$. From the plotted points in Fig. 2, the value of $K$ was evaluated at each annealing temperature by the least-squares method. The evaluated values of $K$ are shown in Fig. 2. Using these values of $K$, $w$ was calculated as a function of $t$ from eq. (2). The results of $T = 973$, 1023 and 1073 K are indicated as dotted, dashed and solid lines, respectively, in Fig. 2.

The ratio $r$ of the thickness $l$ to the migration distance $w$ is defined as

$$r = l/w. \tag{3}$$

The values of $r$ are plotted against the annealing time $t$ in Fig. 3. In this figure, the ordinate shows the ratio $r$, and the abscissa indicates the logarithm of the annealing time $t$. Open triangles, squares and circles show the results of $T = 973$, 1023 and 1073 K, respectively. As can be seen, the ratio $r$ takes values between 0.03 and 0.08 under the present annealing conditions. Although the plotted points are slightly scattered in Fig. 3, various straight lines indicate that $r$ is a monotonically decreasing function of $t$. Consequently, we may conclude that the thickness $l$ is much smaller than the migration distance $w$ even at longer annealing times.

The values of $K$ are plotted against the annealing temperature $T$ as open circles in Fig. 4. In this figure, the ordinate shows the logarithm of $K$, and the abscissa indicates the reciprocal of $T$. If the temperature dependence of $K$ is expressed by the equation

$$K = K_0 \exp(-Q_K/RT), \tag{4}$$

the pre-exponential factor $K_0$ and the activation enthalpy $Q_K$ are evaluated to be $3.01 \times 10^{-3}$ $m^2/s$ and 127 kJ/mol, respectively, from the open circles in Fig. 4 by the least-squares method. Here, $R$ is the gas constant. Using these parameters, $K$ was calculated as a function of $T$ from eq. (4). The result is shown as a solid line in Fig. 4.

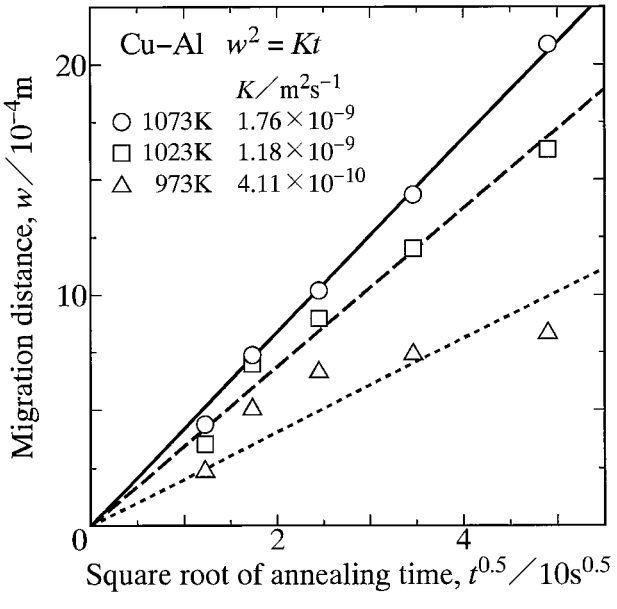


Fig. 2 The migration distance $w$ of the $L/\varepsilon$ interface versus the square root of the annealing time $t$ shown as open triangles, squares and circles at $T = 973$, 1023 and 1073 K, respectively. Straight lines indicate the calculations from eq. (2).

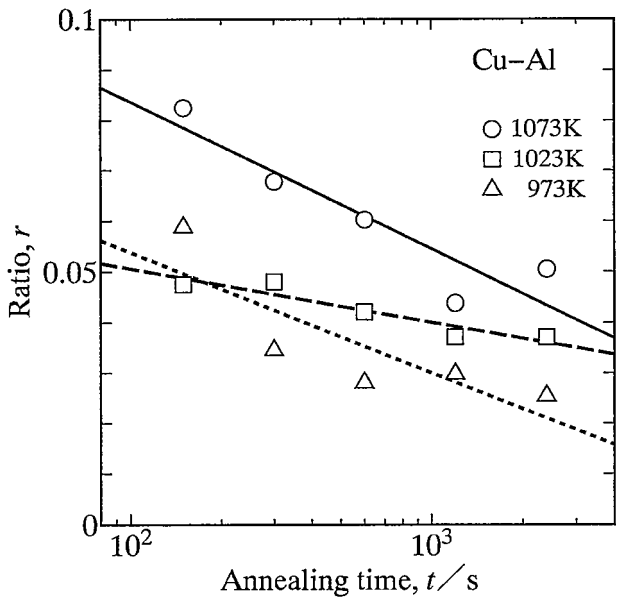


Fig. 3 The ratio $r$ versus the annealing time $t$ shown as open triangles, squares and circles at $T = 973$, 1023 and 1073 K, respectively.

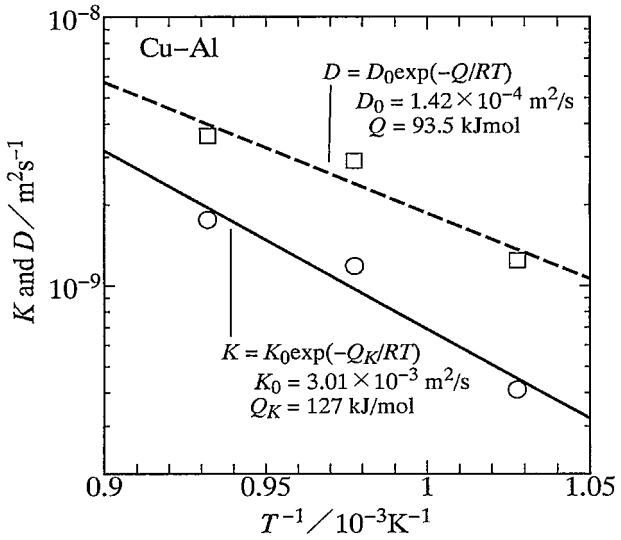


Fig. 4 The parabolic coefficient $K$ versus the reciprocal of the annealing temperature $T$ shown as open circles. The evaluations for the interdiffusion coefficient $D$ of the $L$ phase are indicated as open squares. Solid and dashed lines show the calculations from eqs. (4) and (17), respectively.

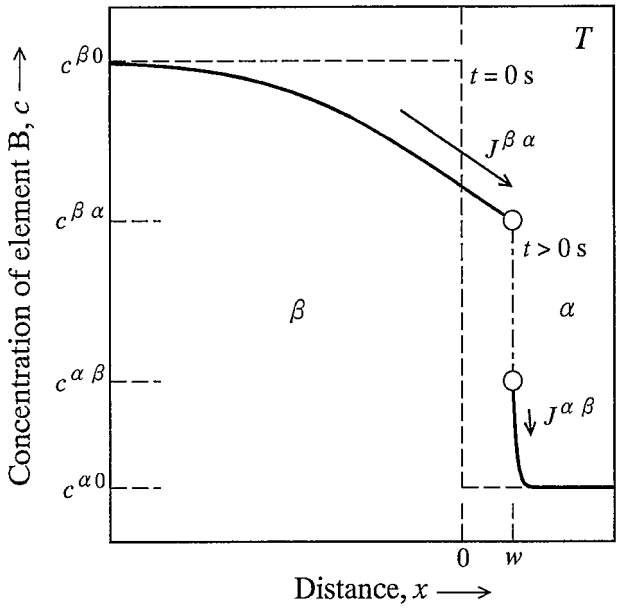


Fig. 5 Concentration profile of element B across the $\alpha/\beta$ interface along the diffusional direction in the semi-infinite diffusion couple.

## 3. Model

As mentioned in Section 2, the thickness $l$ of the intermetallic layer is much smaller than the migration distance $w$ of the $L/\varepsilon$ interface. This means that interdiffusion occurs less remarkably in the $\alpha$, $\beta$, $\gamma$ and $\varepsilon$ phases than in the $L$ phase. In such a case, the migration rate of the $L/\varepsilon$ interface is predominantly determined by the interdiffusion in the $L$ phase, and thus can be described by a simple mathematical model. This model will be explained briefly below.

Let us consider a semi-infinite diffusion couple composed of the $\alpha$ and $\beta$ phases with initial compositions of $c^{\alpha 0}$ and $c^{\beta 0}$, respectively. Here, the $\alpha$ and $\beta$ phases are the A-rich and B-rich phases, respectively, in a binary A–B system, and $c$ is the concentration of element B measured in mol per unit volume. In the semi-infinite diffusion couple, the thickness is semi-infinite for the $\alpha$ and $\beta$ phases, and the $\alpha/\beta$ interface is flat. Therefore, the interdiffusion of elements A and B occurs unidirectionally along the direction perpendicular to the flat interface. This direction is called the diffusional direction. If the diffusion couple is annealed at temperature $T$ for an appropriate time, the $\alpha/\beta$ interface will migrate towards the $\alpha$ or $\beta$ phase depending on the flux balance at the interface. The concentration profile of element B along the diffusional direction across the $\alpha/\beta$ interface is schematically drawn in Fig. 5. In this figure, the ordinate shows the concentration $c$, and the abscissa indicates the distance $x$ measured from the initial position of the $\alpha/\beta$ interface. When the migration of the $\alpha/\beta$ interface is controlled by the volume diffusion in the $\alpha$ and $\beta$ phases and the molar volumes of these phases are equivalent each other, the migration rate $\mathrm{d}w/\mathrm{d}t$ of the interface is related to the flux balance at the interface by the equation[39)]

$$(c^{\beta\alpha} - c^{\alpha\beta})\frac{\mathrm{d}w}{\mathrm{d}t} = J^{\beta\alpha} - J^{\alpha\beta}. \tag{5}$$

Here, $w$ is the migration distance of the $\alpha/\beta$ interface measured from the origin of the distance $x$, $c^{\alpha\beta}$ and $c^{\beta\alpha}$ are the compositions of the $\alpha$ and $\beta$ phases, respectively, at the interface, and $J^{\alpha\beta}$ and $J^{\beta\alpha}$ are the diffusional fluxes of element B due to the volume diffusion in the $\alpha$ and $\beta$ phases, respectively, at the interface. According to Fick's first law, the diffusional flux $J^\theta$ is proportional to the concentration gradient $\partial c^\theta/\partial x$ as follows.

$$J^\theta = -D^\theta \frac{\partial c^\theta}{\partial x} \quad (\theta = \alpha, \beta) \tag{6}$$

In eq. (6), $D^\theta$ is the interdiffusion coefficient for the volume diffusion in the $\theta$ phase, where $\theta$ stands for $\alpha$ and $\beta$. When the interdiffusion coefficient $D^\theta$ is independent of the composition of the $\theta$ phase, Fick's second law is expressed as follows.

$$\frac{\partial c^\theta}{\partial t} = D^\theta \frac{\partial^2 c^\theta}{\partial x^2} \quad (\theta = \alpha, \beta) \tag{7}$$

Equation (7) shows that the composition $c^\theta$ is a function of the distance $x$ and the annealing time $t$. For the semi-infinite $\alpha/\beta$ diffusion couple, the initial conditions are described as

$$c^\alpha(x > 0, t = 0) = c^{\alpha 0} \tag{8a}$$

and

$$c^\beta(x < 0, t = 0) = c^{\beta 0}, \tag{8b}$$

and the boundary conditions are expressed by the equations

$$c^\alpha(x = w, t > 0) = c^{\alpha\beta}, \tag{9a}$$

$$c^\beta(x = w, t > 0) = c^{\beta\alpha}, \tag{9b}$$

$$c^\alpha(x = +\infty, t > 0) = c^{\alpha 0} \tag{9c}$$

and

$$c^\beta(x = -\infty, t > 0) = c^{\beta 0}. \tag{9d}$$

Under these initial and boundary conditions, eqs. (5)–(7) are solved analytically. If $D^{\alpha}$ is much smaller than $D^{\beta}$, $J^{\alpha\beta}$ becomes negligible compared with $J^{\beta\alpha}$ according to eq. (6) unless $\partial c^{\beta}/\partial x$ is much smaller than $\partial c^{\alpha}/\partial x$. In such a case, the following equation is obtained from eqs. (5) and (6).

$$(c^{\beta\alpha} - c^{\alpha\beta})\frac{\mathrm{d}w}{\mathrm{d}t} = J^{\beta\alpha} = -D^{\beta}\left.\frac{\partial c^{\beta}}{\partial x}\right|_{x=w} \tag{10}$$

For the migration of the $\alpha/\beta$ interface controlled by the volume diffusion, the migration distance $w$ is expressed as a function of the annealing time $t$ by the equation[39)]

$$w = K_w\sqrt{4D^{\beta}t}. \tag{11}$$

Here, $K_w$ is the dimensionless coefficient. The coefficient $K_w$ is related with the initial and boundary conditions in eqs. (8) and (9) as follows.[39)]

$$\frac{\exp\{-(K_w)^2\}}{K_w\{1+\mathrm{erf}(K_w)\}} = \frac{c^{\beta\alpha} - c^{\alpha 0}}{c^{\beta 0} - c^{\beta\alpha}}\sqrt{\pi} \tag{12}$$

On the other hand, the following equation is obtained from eqs. (2) and (11).

$$w^2 = 4D^{\beta}(K_w)^2 t = Kt \tag{13}$$

Equation (13) shows that the parabolic coefficient $K$ is expressed as a function of the interdiffusion coefficient $D^{\beta}$ of the $\beta$ phase and the dimensionless coefficient $K_w$ by the equation

$$K = 4D^{\beta}(K_w)^2. \tag{14}$$

Since $K_w$ is dimensionless, the dimension of $K$ corresponds with that of $D^{\beta}$ according to eq. (14). Furthermore, $K_w$ is a function of $c^{\alpha 0}$, $c^{\beta\alpha}$ and $c^{\beta 0}$ through eq. (12), and hence $K$ becomes a function of $c^{\alpha 0}$, $c^{\beta\alpha}$, $c^{\beta 0}$ and $D^{\beta}$ via eq. (14). Thus, $D^{\beta}$ is an inverse function of $c^{\alpha 0}$, $c^{\beta\alpha}$, $c^{\beta 0}$ and $K$. Consequently, $D^{\beta}$ can be evaluated from the value of $K$ determined experimentally for given values of $c^{\alpha 0}$, $c^{\beta\alpha}$ and $c^{\beta 0}$.

## 4. Results and Discussion

### 4.1 Evaluation of interdiffusion

In the mathematical model mentioned in Section 3, the composition is described with the concentration $c$ of element B measured in mol per unit volume. On the other hand, the mol fraction $y$ of element B is practically used to express the composition of each phase. However, the mol fraction $y$ is readily converted into the concentration $c$ by the equation $c = y/V_{\mathrm{m}}$. Here, $V_{\mathrm{m}}$ is the molar volume of the relevant phase. When the molar volume $V_{\mathrm{m}}$ is constant independently of the composition at each annealing temperature, the concentrations $c^{\alpha 0}$, $c^{\beta\alpha}$ and $c^{\beta 0}$ in eq. (12) are automatically replaced with the mol fractions $y^{\alpha 0}$, $y^{\beta\alpha}$ and $y^{\beta 0}$, respectively. Here, the superscript of the mol fraction $y$ possesses the same meaning as the concentration $c$. In the schematic concentration profile of Fig. 5, the diffusional flux $J^{\theta}$ is much greater in the $\beta$ phase than in the $\alpha$ phase, and thus the $\alpha/\beta$ interface migrates towards the $\alpha$ phase. Consequently, the Cu-rich $\alpha$ and Al-rich $L$ phases in the Cu/Al diffusion couple correspond to the $\alpha$ and $\beta$ phases, respectively, for the mathematical model in Section 3. However, the $L$ phase is actually in equilibrium with the $\varepsilon$ phase at each annealing temperature, and thus the liquidus composition corresponds to the mol fraction $y^{L\varepsilon}$ of the $L$ phase for the $L+\varepsilon$ two-phase tie-line. As a result, we obtain the following equation.

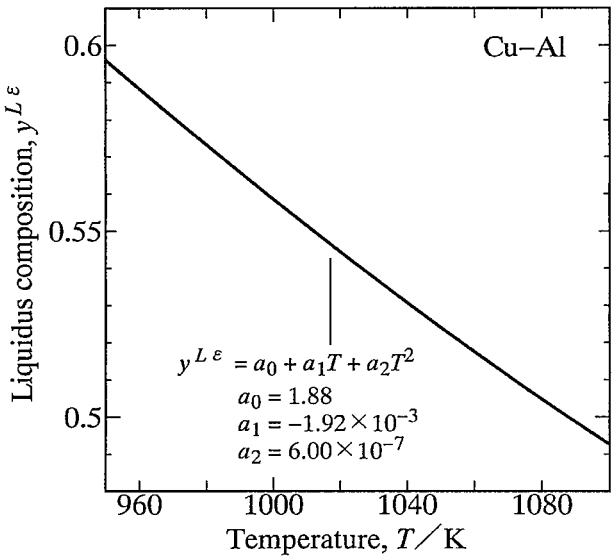


Fig. 6 The liquidus composition $y^{L\varepsilon}$ versus the temperature $T$.[37)]

$$(y^{L\varepsilon} - y^{\alpha 0})\sqrt{\pi}\{1+\mathrm{erf}(K_w)\}K_w - (y^{L0} - y^{L\varepsilon})\exp\{-(K_w)^2\} = 0 \tag{15}$$

Here, $y^{\alpha 0}$ and $y^{L0}$ are the initial compositions of the $\alpha$ and $L$ phases, respectively. From eq. (15), $K_w$ is calculated for given values of $y^{\alpha 0}$, $y^{L\varepsilon}$ and $y^{L0}$. Since $K_w$ is an implicit function of $y^{\alpha 0}$, $y^{L\varepsilon}$ and $y^{L0}$, however, the calculation cannot be carried out in an explicit manner. Therefore, Newton-Raphson's method[40)] was used to calculate numerically the value of $K_w$ from eq. (15). According to a recent phase diagram in the binary Cu–Al system,[37)] $y^{L\varepsilon} = 0.579$, 0.542 and 0.509 at $T = 973$, 1023 and 1073 K, respectively. If the temperature dependence of the composition $y^{L\varepsilon}$ is described by the equation[36)]

$$y^{L\varepsilon} = a_0 + a_1T + a_2T^2, \tag{16}$$

the following values are obtained: $a_0 = 1.88$, $a_1 = -1.92\times10^{-3}$ and $a_2 = 6.00\times10^{-7}$. Using these parameters, the temperature dependence of $y^{L\varepsilon}$ was calculated from eq. (16). The result is shown as a solid curve in Fig. 6. Furthermore, $y^{\alpha 0} = 0$ and $y^{L0} = 1$ for the Cu/Al diffusion couple. For these values of $y^{\alpha 0}$, $y^{L\varepsilon}$ and $y^{L0}$, the calculation provides $K_w = 0.288$, 0.319 and 0.349 at $T = 973$, 1023 and 1073 K, respectively. On the other hand, as shown in Fig. 2, $K = 4.11\times10^{-10}$, $1.18\times10^{-9}$ and $1.76\times10^{-9}$ m$^2$/s were experimentally determined at $T = 973$, 1023 and 1073 K, respectively. Inserting these values of $K$ and $K_w$ into eq. (14), we finally obtain $D = 1.24\times10^{-9}$, $2.91\times10^{-9}$ and $3.62\times10^{-9}$ m$^2$/s at $T = 973$, 1023 and 1073 K, respectively, for the $L$ phase in the binary Cu–Al system. The values of $D$ are plotted against the reciprocal of $T$ as open squares in Fig. 4. The temperature dependence of $D$ is usually described by the following equation of the same formula as eq. (4).

$$D = D_0\exp(-Q/RT) \tag{17}$$

Here, $D_0$ is the pre-exponential factor, and $Q$ is the activation

enthalpy. From the open squares in Fig. 4, $D_0 = 1.42 \times 10^{-4}\,\mathrm{m^2/s}$ and $Q = 93.5\,\mathrm{kJ/mol}$ are evaluated by the least-squares method. Using these parameters, $D$ was calculated as a function of $T$ from eq. (17). The result is shown as a dashed line in Fig. 4. As can be seen, the absolute value is slightly greater for $D$ than for $K$ at each annealing temperature. Sometimes, $D$ may be roughly estimated from $K$ by the equation

$$D = fK, \tag{18}$$

where $f$ takes a constant value of 1, 0.5 or 0.25. This estimation insists that $D$ is not greater than $K$. However, $D$ is greater than $K$ in Fig. 4, and thus $f$ is greater than unity in eq. (18). Furthermore, $Q$ is smaller than $Q_K$, and hence $f$ varies depending on the temperature. Therefore, there is no adequate way to estimate the temperature dependence of $f$. Consequently, the interdiffusion coefficient $D$ cannot be necessarily estimated only from the parabolic coefficient $K$ in a straightforward manner.

The temperature dependence of the tracer diffusion coefficient $D_i^*$ ($i$ = Cu, Al) is also expressed by the equation of the same formula as eq. (17) with the pre-exponential factor $D_{i0}^*$ and the activation enthalpy $Q_i^*$. Unfortunately, however, reliable information is not available for $D_{\mathrm{Al}0}^*$ and $Q_{\mathrm{Al}}^*$ of the tracer diffusion coefficient $D_{\mathrm{Al}}^*$ of Al in the $L$ phase of pure Cu. On the other hand, Ejima and co-workers[41] determined values of $D_{\mathrm{Cu}0}^* = 1.05 \times 10^{-7}\,\mathrm{m^2/s}$ and $Q_{\mathrm{Cu}}^* = 23.8\,\mathrm{kJ/mol}$ for the tracer diffusion coefficient $D_{\mathrm{Cu}}^*$ of Cu in the $L$ phase of pure Al. Using these values of $D_{\mathrm{Cu}0}^*$ and $Q_{\mathrm{Cu}}^*$, $D_{\mathrm{Cu}}^*$ was calculated as a function of the temperature $T$ from eq. (17). The result is shown as a dashed line in Fig. 7. In this figure, the ordinate indicates the logarithm of $D_{\mathrm{Cu}}^*$, and the abscissa shows the reciprocal of $T$. The dashed line for $D$ in Fig. 4 is indicated again as a solid line in Fig. 7. As can be seen, $D$ is close to $D_{\mathrm{Cu}}^*$ at $T = 973$–$1073\,\mathrm{K}$.

The solid-state reactive diffusion in the binary Cu–Al system was experimentally observed using Al/Cu/Al diffusion couples by Funamizu and Watanabe.[42] In their experiment, the diffusion couple was isothermally annealed at temperatures between $T = 673$ and 808 K. During annealing, compound layers of the $\gamma$, $\delta$, $\zeta$, $\eta$ and $\theta$ phases are formed at each interface in the diffusion couple. According to the observation, the parabolic relationship holds good between the mean thickness of each compound layer and the annealing time. This means that the growth of the compound layer is controlled by volume diffusion. From the experimental values of the parabolic coefficient at various annealing temperatures, the temperature dependence of the interdiffusion coefficient was estimated for each compound. The estimation gives $D_0^\gamma = 8.5 \times 10^{-5}\,\mathrm{m^2/s}$ and $Q^\gamma = 136\,\mathrm{kJ/mol}$ as the pre-exponential factor and the activation enthalpy, respectively, of the interdiffusion coefficient $D^\gamma$ for the $\gamma$ phase.[42] The temperature dependence of $D^\gamma$ with these parameters is shown as a thin dashed line in Fig. 7. Since the $\beta$ and $\varepsilon$ phases are not stable at $T = 673$–$808\,\mathrm{K}$,[37] the interdiffusion coefficient was not determined for these compounds in their experiment. On the other hand, the pre-exponential factor $D_{\mathrm{Al}0}^{s*}$ and the activation enthalpy $Q_{\mathrm{Al}}^{s*}$ of the tracer diffusion coefficient $D_{\mathrm{Al}}^{s*}$ of Al in pure Cu were reported as follows: $D_{\mathrm{Al}0}^{s*} = 1.31 \times 10^{-5}\,\mathrm{m^2/s}$ and $Q_{\mathrm{Al}}^{s*} = 185\,\mathrm{kJ/mol}$.[43] The temperature dependence of $D_{\mathrm{Al}}^{s*}$ with these parameters is shown as a thin dotted line in Fig. 7. As can be seen, both $D_{\mathrm{Al}}^{s*}$ and $D^\gamma$ are much smaller than $D$. Hence, we may expect that the interdiffusion coefficient is much smaller also for the $\beta$ and $\varepsilon$ phases than for the $L$ phase. Consequently, it is concluded that the diffusional flux is much smaller in the $\alpha$, $\beta$, $\gamma$ and $\varepsilon$ phases than in the $L$ phase during reactive diffusion in the Cu/Al diffusion couple at $T = 973$–$1073\,\mathrm{K}$. This is the reason why the $L/\varepsilon$ interface migrates towards the $\varepsilon$ phase and the migration rate of the interface is much greater than the growth rates of the $\beta$, $\gamma$ and $\varepsilon$ layers.

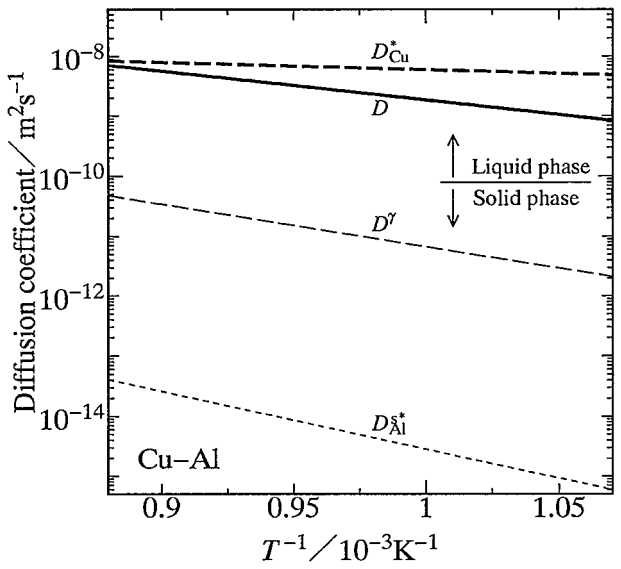


Fig. 7 Various diffusion coefficients versus the reciprocal of the temperature $T$ shown as different straight lines.

### 4.2 Penetration depth of interdiffusion

At each annealing temperature, the mol fraction $y$ of Al in the $L$ phase is expressed as a function of the distance $x$ and the annealing time $t$ by the following equation.[39]

$$y = y^{L0} + \frac{y^{L\varepsilon} - y^{L0}}{1 + \mathrm{erf}(K_w)} \left\{ 1 + \mathrm{erf}\left( \frac{x}{\sqrt{4Dt}} \right) \right\}, \quad x < w \tag{19}$$

Here, $x$ is measured from the initial position of the Cu/Al interface in the diffusion couple. From eq. (19), $y$ was calculated as a function of $x$ for the longest annealing time of $t = 2.4 \times 10^3\,\mathrm{s}$ (40 min) using the following parameters as well as $y^{L0} = 1$ and the value of $y^{L\varepsilon}$ obtained from eq. (16): $K_w = 0.288$ and $D = 1.24 \times 10^{-9}\,\mathrm{m^2/s}$ at $T = 973\,\mathrm{K}$; $K_w = 0.319$ and $D = 2.91 \times 10^{-9}\,\mathrm{m^2/s}$ at $T = 1023\,\mathrm{K}$; and $K_w = 0.349$ and $D = 3.62 \times 10^{-9}\,\mathrm{m^2/s}$ at $T = 1073\,\mathrm{K}$. The results of $T = 973$, 1023 and 1073 K are shown as thin dashed curves in Fig. 8(a), (b) and (c), respectively. In this figure, the ordinate and the abscissa indicate the mol fraction $y$ and the distance $x$, respectively. As long as $y$ is equal to $y^{L0}$ at $x = x_s$, the Cu/Al diffusion couple is considered semi-infinite during annealing. Here, $x_s$ is the position of the flat surface of the $L$ phase parallel to the interface. The initial thickness of the $L$ phase is 4.8 mm and the $L$ phase is initially located on the negative side of $x$ in Fig. 8, and thus $x_s$ is equal to $-4.8$ mm. As can be seen in Fig. 8, however, the penetration depth of

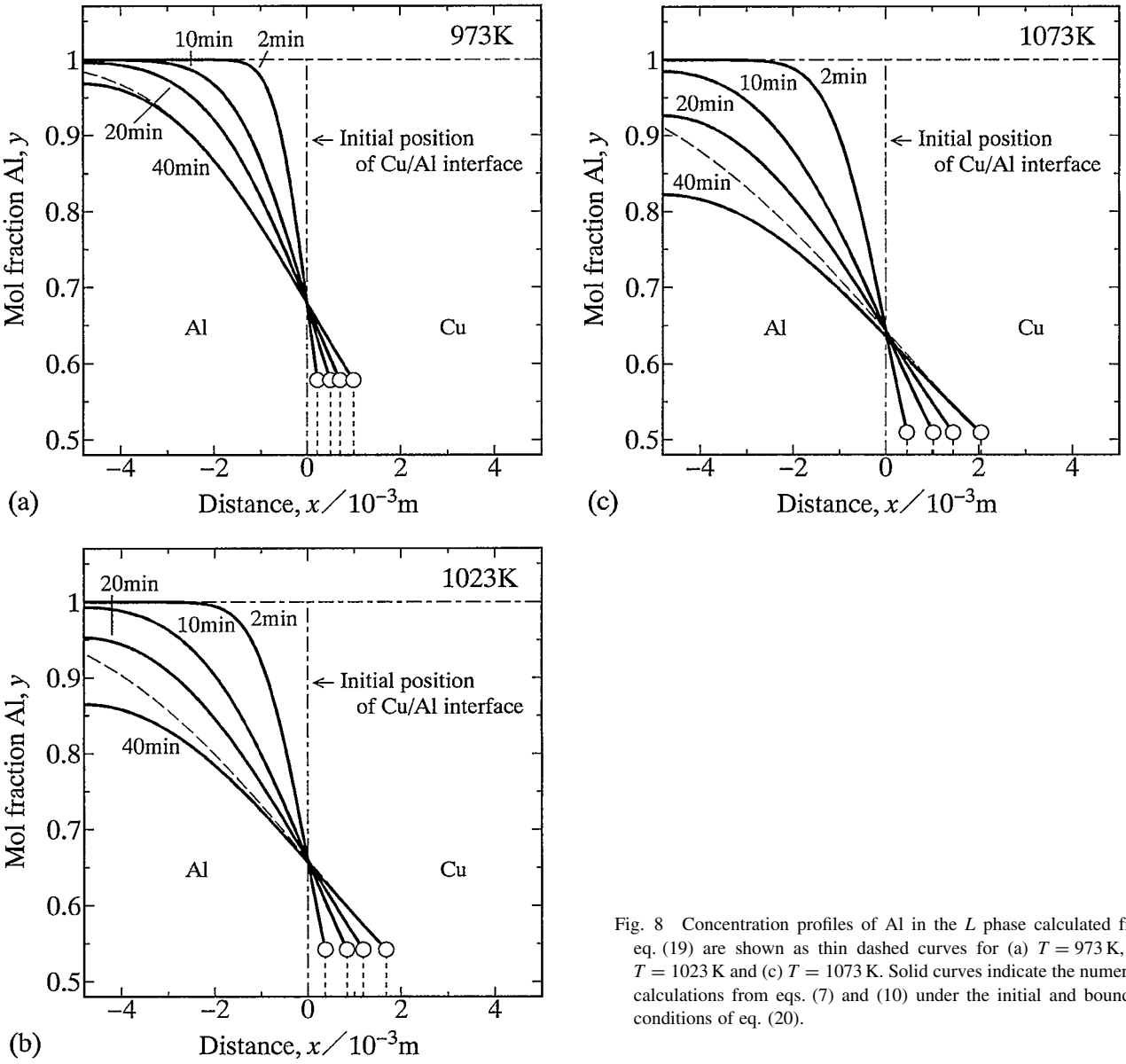


Fig. 8 Concentration profiles of Al in the $L$ phase calculated from eq. (19) are shown as thin dashed curves for (a) $T = 973$ K, (b) $T = 1023$ K and (c) $T = 1073$ K. Solid curves indicate the numerical calculations from eqs. (7) and (10) under the initial and boundary conditions of eq. (20).

interdiffusion in the $L$ phase exceeds the thickness of the $L$ phase at $t = 2.4 \times 10^3$ s (40 min) for all the annealing temperatures, and hence $y$ becomes smaller than $y^{L0}$ at $x = x_s$. Consequently, at the longest annealing time, the Cu/Al diffusion couple is no longer semi-infinite. In such a case, eq. (19) is not applicable. In order to calculate the concentration profile in the $L$ phase for various annealing times up to the longest time, eqs. (7) and (10) were solved numerically under the following initial and boundary conditions:

$$y^L(x < 0, t = 0) = y^{L0}, \tag{20a}$$

$$y^L(x = w, t > 0) = y^{L\varepsilon}, \tag{20b}$$

$$y^\alpha(x = w, t > 0) = y^{\alpha 0} \tag{20c}$$

and

$$\left.\frac{\partial y^L}{\partial x}\right|_{x=x_s} = 0. \tag{20d}$$

In the present numerical calculation, Crank-Nicolson implicit method[44] was combined with a finite-difference technique.[45] The results of $T = 973$, 1023 and 1073 K are shown as bold solid curves in Fig. 8(a), (b) and (c), respectively. Open circles indicate the composition and the position of the interface at different annealing times. At $T = 973$ K in Fig. 8(a), the penetration depth is smaller than the thickness of the $L$ phase at $t = 1.2 \times 10^2$ and $6.0 \times 10^2$ s (2 and 10 min) but greater than that of the $L$ phase at $t = 1.2 \times 10^3$ and $2.4 \times 10^3$ s (20 and 40 min). In contrast, at $T = 1023$ and 1073 K in Fig. 8(b) and (c), the penetration depth outstrips the thickness of the $L$ phase even at $t = 6.0 \times 10^2$ s (10 min). The annealing time dependence of the mol fraction $y_s$ at $x = x_s$ was deduced from the numerical calculation in Fig. 8. The results of $T = 973$, 1023 and 1073 K are shown as dotted, dashed and solid curves, respectively, in Fig. 9. In this figure, the ordinate indicates the mol fraction $y_s$, and the abscissa shows the square root of the annealing time $t$. As can be seen, $y_s$ is equal to $y^{L0}$ at short annealing times. In this case, the Cu/Al diffusion couple is considered semi-infinite. At long annealing times, however, $y_s$ becomes smaller than $y^{L0}$, and hence the diffusion couple is no longer semi-infinite.

If the Cu/Al diffusion couple is not semi-infinite, the

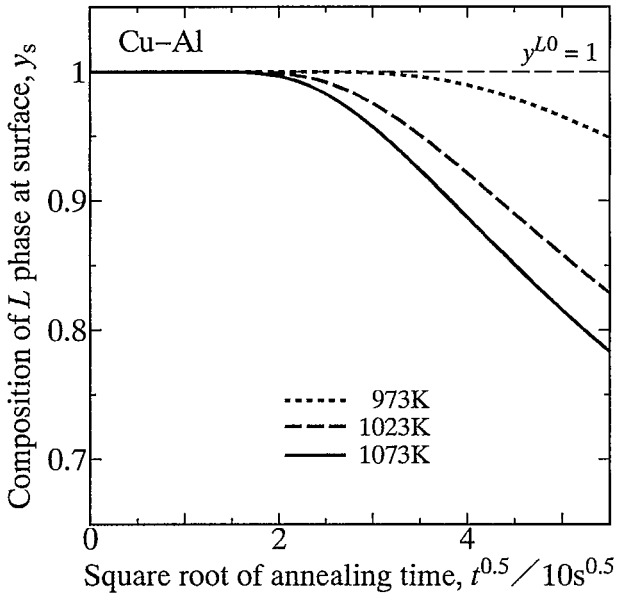


Fig. 9 The composition $y_s$ at $x = x_s$ versus the square root of the annealing time $t$ for the numerical calculation in Fig. 8 shown as dotted, dashed and solid curves at $T = 973$, 1023 and 1073 K, respectively.

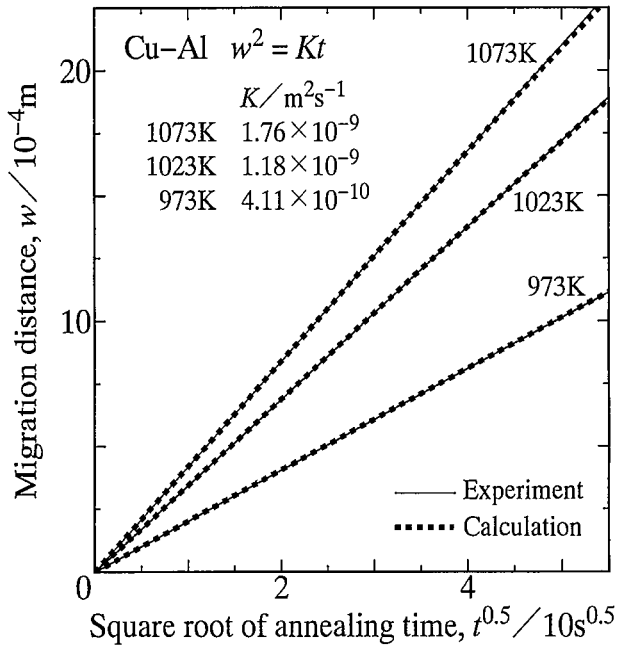


Fig. 10 Straight lines in Fig. 2 are represented as thin solid lines. The corresponding results deduced from the numerical calculation in Fig. 8 are shown as bold dotted curves.

parabolic relationship may not hold good even for the migration of the interface controlled by volume diffusion. Nevertheless, most of the plotted points at each annealing temperature are located well on the corresponding straight line in Fig. 2. The straight lines in Fig. 2 are indicated again as thin solid lines in Fig. 10. On the other hand, the relationship between the migration distance $w$ and the annealing time $t$ was derived from the numerical calculation in Fig. 8. The results of $T = 973$, 1023 and 1073 K are shown as bold dotted curves in Fig. 10. As can be seen, the dotted curve coincides well with the solid line at $T = 973$ K. Also at $T = 1023$ and 1073 K, the dotted curves mostly consist with the corresponding solid lines. As shown in Fig. 8(a), at $T = 973$ K, the dashed curve agrees with the solid curve of $t = 2.4 \times 10^3$ s (40 min) except at small values of $x$. Even at $T = 1023$ and 1073 K, the dashed curves accord with the solid curves of $t = 2.4 \times 10^3$ s (40 min) in the neighborhood of the interface as indicated in Fig. 8(b) and (c), respectively. In Fig. 8, the dashed and solid curves show the concentration profiles for the semi-infinite and finite diffusion couples, respectively. According to eq. (10), the migration rate of the interface is determined by the concentration gradient in the $L$ phase at the interface. As can be seen in Fig. 8, the concentration gradient at the interface is mostly equivalent for the semi-infinite and finite diffusion couples even at the longest annealing time. Therefore, almost the same migration rate of the interface is realized in both diffusion couples under the present annealing conditions. This is the reason why the parabolic relationship holds good within experimental uncertainty also at the long annealing times where the diffusion couple is no longer semi-infinite. When migration of an interface is controlled by volume diffusion in a semi-infinite diffusion couple, the migration surely obeys the parabolic relationship. However, the present numerical calculation indicates that the parabolic relationship holds good even for a finite diffusion couple as long as volume diffusion is the rate-controlling process and the penetration depth of interdiffusion merely slightly eclipses the thickness of each specimen in the diffusion couple.

## 5. Conclusions

The kinetics of the reactive diffusion in the binary Cu–Al system was experimentally observed in a previous study.[28] In that experiment, Cu/Al diffusion couples initially consisting of pure Cu and Al were isothermally annealed at temperatures of $T = 973$–1073 K. At these temperatures, Cu is solid, but Al is liquid. During annealing, compound layers of the $\beta$, $\gamma$ and $\varepsilon$ phases[37] are formed between the Cu-rich solid ($\alpha$) phase and the Al-rich liquid ($L$) phase in the diffusion couple. Furthermore, the $L/\varepsilon$ interface migrates towards the $\varepsilon$ phase. Between the migration distance $w$ of the $L/\varepsilon$ interface and the annealing time $t$, there exists the parabolic relationship $w^2 = Kt$, where $K$ is the parabolic coefficient. The observation provides $K = 4.11 \times 10^{-10}$, $1.18 \times 10^{-9}$ and $1.76 \times 10^{-9}$ m$^2$/s at $T = 973$, 1023 and 1073 K, respectively. The total thickness $l$ of the compound layers is much smaller than the migration distance $w$. This means that the migration of the $L/\varepsilon$ interface is predominantly controlled by the volume diffusion in the $L$ phase. In order to evaluate the interdiffusion coefficient $D$ of the $L$ phase, the experimental results were mathematically analyzed using the diffusion equation describing the flux balance at the migrating interface.[39] The analysis deduces $D = 1.24 \times 10^{-9}$, $2.91 \times 10^{-9}$ and $3.62 \times 10^{-9}$ m$^2$/s at $T = 973$, 1023 and 1073 K, respectively. When the temperature dependence of $D$ is expressed by the equation $D = D_0 \exp(-Q/RT)$, values of $D_0 = 1.42 \times 10^{-4}$ m$^2$/s and $Q = 93.5$ kJ/mol are obtained by the least-squares method. According to the analysis, the interdiffusion occurs much faster in the $L$ phase than in the solid phases. This is the

reason why the $L/\varepsilon$ interface migrates towards the $\varepsilon$ phase and the migration rate of the interface is much greater than the overall growth rate of the compound layers.

## Acknowledgements

The present study was supported by a Grant-in-Aid for Scientific Research from the Ministry of Education, Culture, Sports, Science and Technology of Japan.

## REFERENCES

1) T. B. Massalski, H. Okamoto, P. R. Subramanian and L. Kacprzak: *Binary Alloy Phase Diagrams* (ASM International, Materials Park, OH, 1990) vol. 1–3.
2) B. Lustman and R. F. Mehl: Trans. Met. Soc. AIME **147** (1942) 369–394.
3) D. Horstmann: Stahl Eisen **73** (1953) 659–665.
4) S. Storchheim, J. L. Zambrow and H. H. Hausner: Trans. Met. Soc. AIME **200** (1954) 269–274.
5) G. V. Kidson and G. D. Miller: J. Nucl. Mater. **12** (1964) 61–69.
6) K. Shibata, S. Morozumi and S. Koda: J. Japan Inst. Met. **30** (1966) 382–388.
7) K. Hirano and Y. Ipposhi: J. Japan Inst. Met. **32** (1968) 815–821.
8) M. M. P. Janssen: Metall. Trans. **4** (1973) 1623–1633.
9) G. F. Bastin and G. D. Rieck: Metall. Trans. **5** (1974) 1817–1826.
10) M. Onishi and H. Fujibuchi: Trans. JIM **16** (1975) 539–547.
11) EI-B. Hannech and C. R. Hall: Mater. Sci. Tech. **8** (1992) 817–824.
12) P. T. Vianco, P. F. Hlava and A. L. Kilgo: J. Electron. Mater. **23** (1994) 583–594.
13) M. Watanabe, Z. Horita and M. Nemoto: Interface Science **4** (1997) 229–241.
14) S. Choi, T. R. Bieler, J. P. Lucas and K. N. Subramanian: J. Electron. Mater. **28** (1999) 1209–1215.
15) M. Kajihara, T. Yamada, K. Miura, N. Kurokawa and K. Sakamoto: Netsushori **43** (2003) 297–298.
16) T. Yamada, K. Miura, M. Kajihara, N. Kurokawa and K. Sakamoto: J. Mater. Sci. **39** (2004) 2327–2334.
17) T. Yamada, K. Miura, M. Kajihara, N. Kurokawa and K. Sakamoto: Mater. Sci. Eng. A **390** (2005) 118–126.
18) K. Suzuki, S. Kano, M. Kajihara, N. Kurokawa and K. Sakamoto: Mater. Trans. **46** (2005) 969–973.
19) M. Mita, M. Kajihara, N. Kurokawa and K. Sakamoto: Mater. Sci. Eng. A **403** (2005) 269–275.
20) T. Takenaka, S. Kano, M. Kajihara, N. Kurokawa and K. Sakamoto: Mater. Sci. Eng. A **396** (2005) 115–123.
21) D. Naoi: Master Eng. Thesis, Tokyo Institute of Technology, 2006.
22) T. Takenaka, M. Kajihara, N. Kurokawa and K. Sakamoto: Mater. Sci. Eng. A **406** (2005) 134–141.
23) T. Takenaka, S. Kano, M. Kajihara, N. Kurokawa and K. Sakamoto: Mater. Trans. **46** (2005) 1825–1832.
24) M. Mita, K. Miura, T. Takenaka, M. Kajihara, N. Kurokawa and K. Sakamoto: Mater. Sci. Eng. B **126** (2006) 37–43.
25) T. Takenaka and M. Kajihara: Mater. Trans. **47** (2006) 822–828.
26) T. Takenaka, M. Kajihara, N. Kurokawa and K. Sakamoto: Mater. Sci. Eng. A **427** (2006) 210–222.
27) Y. Yato and M. Kajihara: Mater. Sci. Eng. A **428** (2006) 276–283.
28) Y. Tanaka, M. Kajihara and Y. Watanabe: Mater. Sci. Eng. A, in press.
29) Y. Yato and M. Kajihara: Mater. Trans. **47** (2006) 2277–2284.
30) Y. Muranishi and M. Kajihara: Mater. Sci. Eng. A **404** (2005) 33–41.
31) T. Hayase and M. Kajihara: Mater. Sci. Eng. A **433** (2006) 83–89.
32) M. Kajihara: Acta Mater. **52** (2004) 1193–1200.
33) M. Kajihara: Mater. Sci. Eng. A **403** (2005) 234–240.
34) M. Kajihara: Mater. Trans. **46** (2005) 2142–2149.
35) M. Kajihara: Defect and Diffusion Forum **249** (2006) 91–95.
36) M. Kajihara: Mater. Trans. **47** (2006) 1480–1484.
37) T. B. Massalski, H. Okamoto, P. R. Subramanian and L. Kacprzak: *Binary Alloy Phase Diagrams* (ASM International, Materials Park, OH, 1990) vol. 1, pp. 141–143.
38) Y. L. Corcoran, A. H. King, N. de Lanerolle and B. Kim: J. Electron. Mater. **19** (1990) 1177–1183.
39) W. Jost: *Diffusion of Solids, Liquids, Gases* (Academic Press, New York, 1960) pp. 68–82.
40) G. Dahlquist and Å. Björck: *Numerical Methods* (Prentice-Hall, Englewood Cliffs, NJ, 1974) pp. 222–224.
41) T. Ejima, T. Yamamura, N. Uchida, Y. Matsuzaki and M. Nikaido: J. Jpn. Inst. Met. **44** (1980) 316–323.
42) Y. Funamizu and K. Watanabe: Trans. Jpn. Inst. Met. **12** (1971) 147–152.
43) *Metals Data Book*, ed. Japan Institute of Metals (Maruzen, Tokyo, 1993) p. 21.
44) J. Crank: *The Mathematics of Diffusion* (Oxford Univ. Press, London, 1979) pp. 144–148.
45) R. A. Tanzilli and R. W. Heckel: Trans. Met. Soc. AIME **242** (1968) 2313–2321.